H.A. ELMELEEGI,[1] Z.S. ELMANDOUH,[1] F. TAHER[2]

[1] Physical Research Division, National Research Center (NRC)
(12622, Dokki, Cairo, Egypt)
[2] Faculty of Science, AlAzhar University(Girls)
(2, Cairo, Egypt)

CARRIER TYPE REVERSAL
OF GRAPHENE MULTILAYERED THIN FILMS

Graphene has unique two-dimensional structure, high surface area, and remarkable chemical stability. Graphene oxide (GO) produced by the Hummers method was reduced to graphene by pulsed laser deposition (PLD). The graphene specimen in the form of a powder and a multilayered structure is studied. X-ray diffraction of graphene is interpreted to elucidate its short-range order and to calculate the number of layers of graphene. Electron diffraction and transmission electron microscope studies elucidate the short-range order nature of deposited graphene. The temperature dependence of the Seebeck coefficient (S) indicates the carrier type reversal (CTR) from the n- to p-type, by starting from 60 °C. CTR is affected by the applied voltage, frequency, and temperature. Distinct oscillations in the Seebeck coefficient thickness dependence are observed and attributed to the size quantization effect in graphene layers. The velocity, mobility, and electrical conductivity are measured and calculated to complete the transport properties of graphene.

K e y w o r d s: structure, carrier type reversal, thermoelectric power, electrical conductivity.

1. Introduction

The graphene properties have been studied due to its unique physics and important applications in many electronic devices [1–8]. The preparation method of graphene affects its properties. Important applications have been done, by using different methods [9, 10]. Graphene is a new condensed promising material with very good physical properties [11–15]. The variation of the preparation methods of graphene allows one to synthesize graphene easily and economically, by using the chemical vapor deposition (CVD) [16], mechanical exfoliation (repeated peeling) of graphite [17], chemical intercalation and exfoliation of graphite [18, 19], and thermal expansion of graphite [20]. The effect of the graphene structure on its physical properties was investigated in [21–22]. The structural and electrical properties of graphene in different forms at different temperatures were studied in [24], by using the four-probe method. It was that the graphene resistivity decreases rapidly with temperature. The effect of the metal interaction that affects the band structure and the binding energy of graphene layers was investigated in [24].

Monolayer and bilayer graphenes [25, 26, 27] are gapless two-dimensional semiconductors [28, 29, 30], whereas three-dimensional graphite is a semimetal [31, 32, 33]. Hence, the dimensionality effects for the unique substance can be studied [34]. Monolayer graphene has a very simple electron band structure. Near the energy ε = zero, the energy bands are cones at the K points in the two-dimensional Brillouin zone with the constant velocity parameter equal to $108\,\mathrm{cm\cdot s^{-1}}$. Such degeneration is conditioned by symmetry. Carbon has four electrons in four hybridized bondings $(2S^1,\ 2P_x^1,\ 2P_y^1,\ 2P_z^1)$ that are able to form covalent chemical bonds. In a two-dimensional graphene, three carbon electrons form strong in-plane SP^2 bonds, making a honey-comb structure, and a fourth electron spreads out over the top or the bottom of the layer as a π electron [35].

2. Experimental Work

Graphene oxide (GO) was synthesized from natural white graphite (Sigma-Aldrich) by a modified Hummers method [36, 37]. The GO paste collected from a filter paper is dispersed in deionized water (600 ml) by ultrasound (70% amplitude for 1 h). The suspension is washed with deionized water $5 \sim 7$ times for five days by decantation. Finally filtered, well-washed GO

paste collected on a filter paper is re-dispersed into water by the ultrasonication. The obtained brown dispersion is then subjected to the centrifugation for 30 min at 5000 rpm to remove any un-exfoliated GO. Graphene oxide was obtained by the dehydration at 60 °C. Afterward, a one-layer graphene film was grown on glass substrates by the pulsed laser deposition technique. One g of dark brown graphene oxide sheets was loaded for the PLD experiment. The energy of a laser destroys the O bonds in graphene oxide, and graphene was precipitated on glass slides [38]. A titanium sapphire femto-second laser with a wavelength of 800 nm, pulse duration of 40 fs, average pulse energy of 220 mW, and maximum repetition rate of 1000 Hz was used. The glass substrates were separated from the target at a distance of approximately 9 cm with a rotation speed of 8 rpm to guarantee a homogeneous consumption for a typical irradiation time of 20 min. The deposition chamber was evacuated to a base pressure of approximately 8.4×10^{-4} Torr. The maximum temperature of the glass substrates was 200 °C. UV/VIS absorption and transmission (normal incidence spectrum) were measured using a T80 + UV/VIS spectrometer (PG Instruments Ltd.), whereas the transmission and electron diffraction measurements were done by a JEOL-TEM model: JEM-1230. To determine the conduction type of graphene, a special circuit was designed. The circuit is operated from a sine wave function generator, the type of conductivity is determined by the shape of volt-ampere characteristics on the oscilloscope screen.

3. Results and Discussion

3.1. Structure

Graphene, as a single atomic layer of sp^2-hybridized carbon arranged in a honeycomb structure, is a two-dimensional allotrope of carbon. The electron micrograph of graphene thin films is presented in Fig. (1, *a*) which shows the layered structure with nanoparticles distributed on its surface. The electron diffraction pattern of a graphene powder demonstrates the short-range order, as it is confirmed by the existence of halo rings seen in Fig. (1, *b*). The specimen investigated by TEM shows nanocrystalline particles with dimensions between 2–4 nanometers disturbed among short-range ordered layers. The X-ray diffraction spectrum of graphene thin film (Fig. (1, *c*)) shows
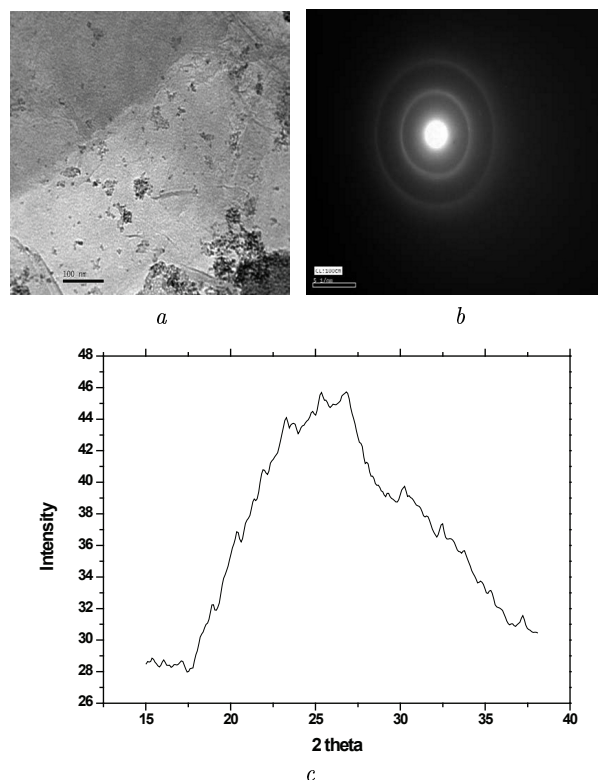

Fig. 1. Transmission electron microscope image for powder multilayered graphene (*a*). Electron diffraction image for powder multilayered graphene (*b*). XRD after the pulsed laser deposition for a thin-film specimen (*c*)

a steep hump at $2\theta = 26$–$27°$ which is characteristic of graphene [39]. The distance between graphene layers can be calculated based on Bragg's law [41], the mean crystallite size can be determined from the Scherrer equation [40, 41].

$$L_{hkl} = \frac{A\lambda}{\beta_0 \cos \phi}. \tag{1}$$

Here, L_{hkl} is the mean dimension of a crystallite perpendicular to $[hkl]$ plane, β_0 is the full width of the peak at half maximum in radiance, and A is a constant equals to 0.89 [42]. The number of graphene layers (N) can be obtained using the relation [42]

$$N = \frac{L_{hkl}}{d_{hkl}}. \tag{2}$$

Here, d is the interspacing between planes of the lattice. The average calculated number of graphene layers was found to be 6 according to relation (2).

4. Thermoelectrical Properties

The thermoelectric data in Fig. 2 reveal that the thin film shows the n-type conduction at room temperature. The conduction type starts to change from n- to p-type at 60 °C. The charge density of graphene can be tuned continuously between electrons and holes, whereas the electron mobility remains high even at
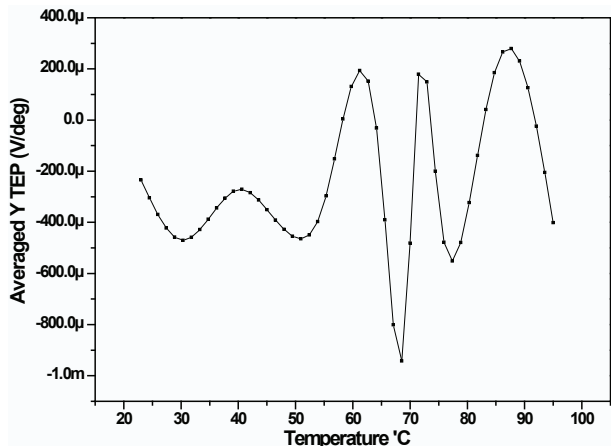

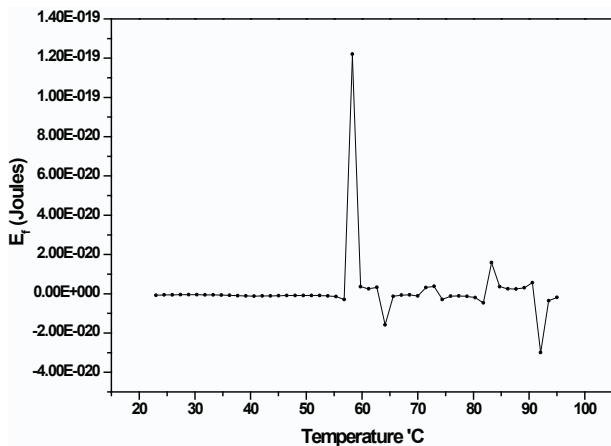**Fig. 2.** Relation between the thermoelectric power and the temperature

Fig. 3. Temperature dependence of the Fermi energy

Temperature dependence of the efficiency of graphene as a thermoelectric energy converter

Temperature, °C	30	50	68.6	77.5	87.7	95
Optimum thermoelectric efficiency, %	51	49	66.8	52.5	31	42.5

high carrier concentrations [43]. The carrier-type reversal is caused by a change in the Fermi-energy level with a change of the temperature, as it is presented in Fig. 3. The Fermi energy can be obtained from the thermoelectric power curve using the relation [44]

$$S = \frac{\pi^2 K}{3e\eta} \left(r + \frac{D}{2} \right).$$ (3)

Here, $\eta = E_F/KT$, E_F is the Fermi energy, K is the Boltzmann constant, T is the temperature in Kelvins, S is the Seebeck thermoelectric power coefficient, q is the electron charge, D is the dimensionality factor equal to 2 for two dimensions, and r is the scattering parameter $= 2/3$ [44]. The Q-factor Z can be determined from [45]

$$Z = \frac{S^2}{\rho\kappa}.$$ (4)

Here, κ is the thermal conductivity, and ρ is the electric resistivity.

The maximum efficiency (Q) can be calculated from the relation [45]

$$Q = \frac{\Delta T}{T_h} \frac{\sqrt{1 + ZT} - 1}{\sqrt{1 + ZT} + \frac{T_c}{T_h}}.$$ (5)

Here, $\Delta T = T_h - T_c$, where T_h is the temperature of the hot end of the specimen, and T_c is the cold end temperature. The data on the temperature dependence of the thermoelectric efficiency is represented in Table [1]. Like all heat engines, the maximum power generation efficiency of a thermoelectric generator is thermodynamically limited by the Carnot efficiency ($\Delta T/T_h$). Combining the substructure approach with the nano-structuring seems to be the most promising method of achieving a high Seebeck coefficient. In the case of a degenerate electron gas, the conductivity [46] can be calculated according to the Mott equation (6)

$$S = \left[\frac{\pi^2 K^2 T}{3e} \right] \left(\frac{\partial Ln(\sigma)}{\partial E_f} \right).$$ (6)

Here, σ is the electrical conductivity. Figure 4, a shows the relation between the conductivity and the temperature obtained according to Eq. (6). This figure indicates the switching from a low resistance value represented by R_{on} to a high resistance value represented by R_{off}, where $R_{on} \ll R_{off}$ ($\sigma_{on} \gg \sigma_{off}$). The
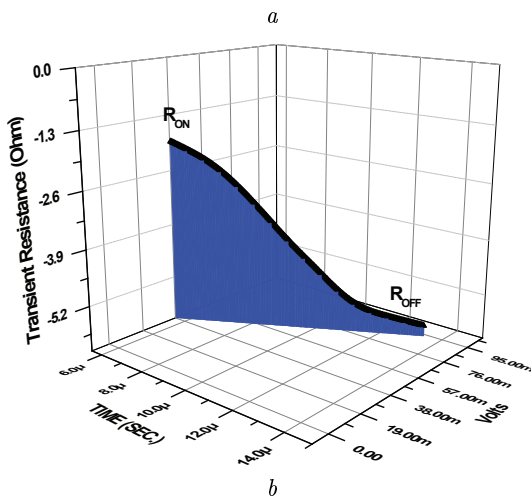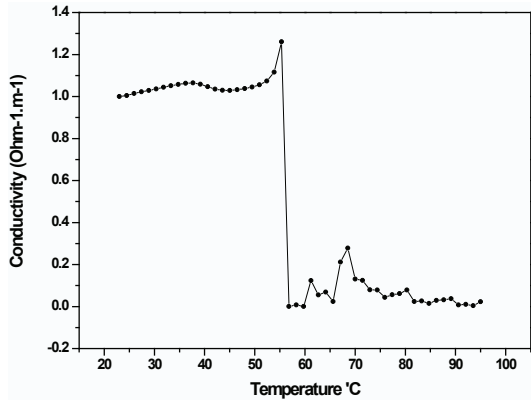
a

b

Fig. 4. Electrical conductivity vs. temperature (*a*). Transient electrical resistance vs. time and applied voltage (*b*)

temperature, at which the switching occurs, is 60 °C that is the same temperature, at which the carrier type reversal from *n*- to *p*-type happens. A model for thermoresistance function for thin films [47] is presented by

$$M(q(t)) = R_{\text{off}}\left(1 - \frac{\mu R_{\text{on}} q(t)}{d^2}\right). \tag{7}$$

The variation of the resistance with the time and the voltage is presented in Fig. 4, *b*. Here, μ is the mobility of carriers in a film, *t* is the time in seconds, and *d* is the film thickness. It is assumed that the oscillatory behavior of the observed dependence of *S* on the thickness shown in Fig. 5 can be attributed to the quantum size effect taking place in graphene layers, when its thickness becomes comparable to the
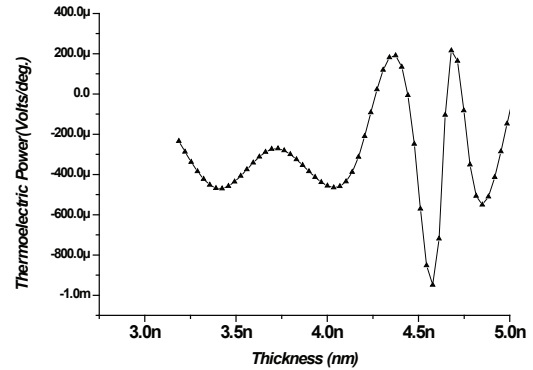

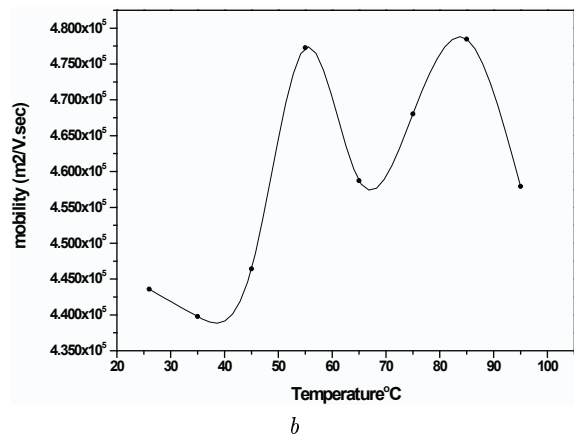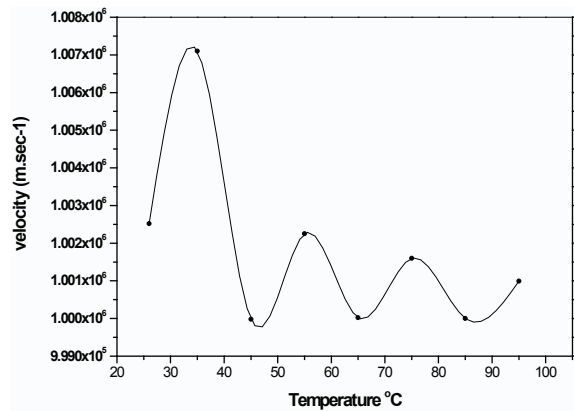**Fig. 5.** Thermoelectric power vs. thickness

a

b

Fig. 6. Drift velocity of charged carriers vs. temperature (*a*). Drift mobility of charged carriers vs. temperature (*b*)

de Broglie wavelength represented as

$$\Delta d = \lambda_{\text{f}}/2 = h/\sqrt{8m^* E_f}. \tag{8}$$

Relation (8) represents a change in the thickness Δd with the Fermi energy level. Calculations of the thick-
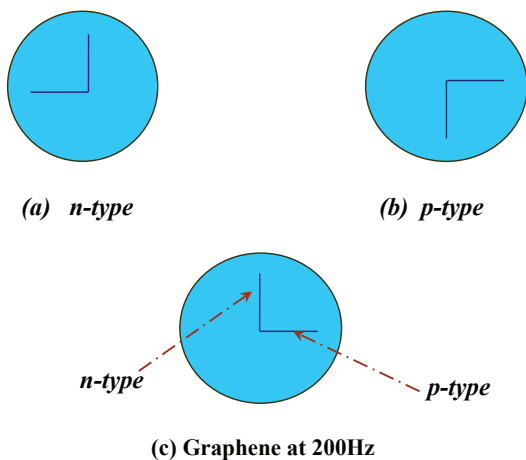
(a) n-type

(b) p-type

(c) Graphene at 200Hz

Fig. 7. Examples of n- and p-type conductivities are shown in (a) and (b). Transition of the conduction from n- to p-type is at 200 Hz (c)

ness were done theoretically from relations (8) and (9) and showed its variation with the temperature from 3 to 5 nm. This change determines the oscillatory behavior of the density of states as a function of (d), which leads to oscillations in the kinetic and thermoelectric characteristics [48]. In order to determine the mobility, we used the following procedure. Voltage V applied to the graphene layer in the source-drain direction causes the visible-light-generated carriers to drift; thereby, it produces a photo-current I_{ph} in the circuit. This current is easy to be determined through an oscilloscope circuit during its life-time; every charge carrier passes τ/t_{dr} times through graphene, where τ is the carrier life-time, and t_{dr} is the transient or drift time of the carrier, which equals

$$t_{dr} = \frac{l}{v_{dr}} = \frac{l}{\mu E} = \frac{l^2}{\mu V}. \tag{9}$$

From this equation, the velocity and, consequently, the mobility of carriers as functions of the temperature are calculated; they are presented in Fig. 6, a, b.

5. Recording the CTR Phenomenon in the Alternative Current Range

A very fascinating experiment [49] was done to reveal the CTR in a graphene layer by changing the frequency applied to it. The oscilloscope record, Fig. 7, a, b, represents the standard n-type and p-type conduction specimens. If the probe of a signal generator is applied to an n-type specimen, a large forward current begins to flow through the metal-semiconductor contact during positive half- cycles causing a considerable voltage drop across the vertical electrodes of a cathode-ray tube. The electron beam is abruptly deflected upward. Since the forward voltage drop and the voltage applied to the horizontal electrodes (connected in parallel to the metal-semiconductor contact) are relatively small, the electron beam traces out a practically straight line upon an oscilloscope screen from the center upward. During the negative half-cycles, the metal-semiconductor contact is connected in the reverse direction, and a small reverse current, which causes only a slight voltage drop across the resistance, flows. Thus, the entire voltage becomes concentrated at the metal-semiconductor contact. The electron beam traces out a horizontal straight line on a screen from the center to the left. Consequently, the image on the oscilloscope in Fig. 7, a represents the voltage-ampere characteristic of the metal-semiconductor contact.

If the specimen is a p-type semiconductor, the reverse and forward directions correspond, respectively, to positive and negative half-cycles. The corresponding straight lines on the oscilloscope screen run in the opposite directions from the screen center, as shown in Fig. 7, b.

Figure 7, c for a graphene multilayered as-prepared film shows a negative upward vertical part, which represents the n-type conduction. A right horizontal part for the graphene specimen represents a positive p-type conduction. This indicates the carrier type reversal in the graphene specimen, where the first half-cycle corresponds to the n-type conduction (as-prepared specimen). Then it turns to the p-type conduction in the second half-cycle at the frequency equal to 200 Hz.

6. Conclusion

The surface morphology of graphene powder is studied, by using TEM and electron diffraction. This study indicates that the graphene specimens are composed of 6 layers with nanoparticles distributed over the short-range ordered structure with dimensions around 2–4 nm. Thermoelectric properties of graphene indicates a carrier type reversal at 60 °C. The curve of the thermoelectric power reveals the oscillatory behavior vs. the temperature and the thickness. The

oscillatory dependence of the thermoelectric properties on the thickness is attributed to the quantum size effect. Conductivity shows the switching behavior (from σ_{on} for high conductivity to σ_{off} at low conductivity) at 60 °C at the CTR point. The carrier type reversal in the ac-range is recorded, by using an oscilloscope special circuit at 200 Hz. The results obtained can be used in the fabrication of a new generation of $p-n$ junctions depending on the carrier type reversal.

1. A.K. Geim and K.S. Novoselov, Nat. Mater. **6**, 183 (2007).
2. N. Tombros, C. Jozsa, M. Popinciuc, H.T. Jonkman, and B.J.V. Wees, Nature **1448**, 571 (2007).
3. J.M. Carlsson, Nat. Mater. **6**, 801 (2007).
4. T. Ramanathan, A.A. Abdala, S. Stankovich, D.A. Dikin, M. Herrera-Alonso, R.D. Pinar, D.H. Adamson, H.C. Schnipp, X. Chen, R.S. Ruoff, and S.T. Nguyen, Nat. Nanotechnol. **3**, 327 (2008).
5. M. Liang and L. Zhi, J. Mater. Chem. **19**, 5871 (2009).
6. S.R.C. Vivekchand, C.S. Rout, K.S. Subrahmanyam, A. Govindaraj, and C.N.R. Rao, J. Chem. Sci. **120**, 9 (2008).
7. J. Zhu, Nat. Nanotechnol. **3**, 528 (2008).
8. S. Patchkovskii, J.S. Tse, S.N. Yurchenko, L. Zhechkov, T. Heine, and G. Seifert, PNAS **102**, 10439 (2005).
9. N.A. Kotov, Nature **442**, 254 (2006).
10. G. Eda and M. Chhowalla, Nano Lett. **9**, 814 (2009).
11. K.S. Novoselov, A.K. Geim, S.V. Morozov, D. Jiang, M.I. Katsnelson, and I.V. Grigorieva, Nature **438**, 197 (2005).
12. Y.B. Zhang, Y. Tan, H.L. Stormer, and P. Kim, Nature **438**, 201 (2005).
13. J.C. Meyer, A.K. Geim, M.I. Katsnelson, K.S. Novoselov, and T.J. Booth, S. Roth. Nature **446**, 9, 60(2007).
14. M.I. Katsnelson and K.S. Novoselov, Solid State Commun. **143**, 3 (2007).
15. F. Schedin, A.K. Geim, S.V. Morozov, E.W. Hill, P. Blake, and M.I. Katsnelson, Nat. Mater. **6**, 652 (2007).
16. A.N. Obraztsov, Nat. Nanotechnol. **4**, 212 (2009).
17. J.C. Meyer, C.O. Girit, M.F. Crommie, and A. Zettl, Nature **454**, 319 (2008).
18. C.T. Vincent, J.A. Matthew, Y. Yang, and B.K. Richard, Nat. Nanotechnol. **4**, 25 (2009).
19. S. Park and R. Ruoff, Nat. Nanotechnol. **4**,217(2009).
20. M.J. McAllister, J. Li, D.H. Adamson, H.C. Schniepp, A.A. Abdala, J. Liu, M. Herrera-Alonso, and D.L. Milius, Chem. Mater. **19**,4396(2007).
21. K.S. Novoselov, A.K. Geim, S.V. Morozov, D. Jiang, Y. Zhang, S.V. Dubonos, I.V. Grigorieva, and A.A. Firsov, Science **306**, 666 (2004).
22. K.I. Bolotin, K.J. Sikes, Z. Jiang, G. Funderberg, J. Hones, P. Kim, and H.L. Stormer, Solid State Commun. **146**, 351 (2008).
23. R. Sanjinés, M.D. Abad, Cr. Vâju, R. Smajda, M. Mionić, and A. Magrez, Surf. & Coat. Techn. **206**, 727 (2011).
24. P.S. Kireev, *Semiconductor Physics* (Mir Publishers, Moscow, 1975).
25. K.S. Novoselov, A.K. Geim, S.V. Morozov, D. Jiang, M.J. Katsnelson, I.V. Grigorieva, S.V. Dubonos, and A.A. Firsov, Science **306**, 666 (2004); Nature **438**, 197 (2005).
26. Y. Zhang, J.P. Small, M.E.S. Amory, and P. Kim, Phys. Rev. Lett. **94**,176803 (2005); Nature **438**, 201 (2005).
27. K.S. Novoselov, E. McCann, S.V. Morozov, V.I. Fal'ko, M.J. Katsnelson, U. Zeitler, D. Jiang, F. Shedin, and A.K. Geim, Nat. Phys. **2**, 177 (2006).
28. M.S. Dresselhaus and G. Dresselhaus, Adv. Phys. **51**, 1 (2002).
29. N. Ando, J. Phys. Soc. Jpn. **74**, 777 (2005).
30. E. McCann and V.I. Fal'ko, Phys. Rev. Lett. **96**, 086805 (2006).
31. P.R. Wallas, Phys. Rev. **71**, 622 (1974).
32. J.C. Slonczewski and P.R. Weiss, Phys. Rev. **99**, 636(A) (1955).
33. J.W. MacClure, Phys. Rev. **104**, 666 (1956).
34. E. Fradkin, Phys. Rev. B **33**, 3263 (1986).
35. S.H. Hun, in: *Physics and Applications of Graphene – Experiments*, edited by S. Mikhailov (InTech, 2011), p.74.
36. W.S. Hummers, R.E. Offeman, J. Am. Chem. Soc. **80**, 1339 (1958).
37. H.A. Becerril, J. Mao, Z.F. Liu, R.M. Stoltenberg, Z.N. Bao, and Y.S. Chen, ACS Nano **2**, 463(2008).
38. L. Huang; Y. Liu, L. Ji, Y.Qun Xie, T. Wang, and W.Z. Shi, Carbon **49**, 2431 (2011).
39. R.J. Seresht, M. Jahanshahi, A. Rashidi, and A.A. Ghoreyshi, Appl. Surf. Sci. **276**, 672 (2013).
40. R.W. James, X-Ray Crystallography (Wiley, New York, 1961).
41. B.D. Cullity, *Elements of X-Ray Diffraction* (Addlson-Wesley, Reading, MA, 1956).
42. H.M. Ju, S.H. Choi, and S.H. Huh, J. of Korean Phys. Society **57**, 1649 (2010).
43. D.A. C.Brawnson, D.K. Kampouris, and C.E. Banks, J. Power Sources **196**, 4873 (2011).
44. P. Pichanuskorn, and P. Bandaru, Mater. Sci. and Engin. **67**, 19 (2010).
45. G.J. Snyder, and E.S. Toberer. Nature Mater. **7**, 105 (2008).
46. K. Seeger, *Semiconductor Physics, an Introduction* (Springer, Berlin, 1997).
47. D.B. Strukov, G.S. Snider, D.R. Stewart, and S.R. Williams, Nature **453** (7191), 80 (2008).

48. B.A. Tavger and V.Ya. Demikhovskii, Usp. Fiz. Nauk **96**, 61 (1968).

49. V.A. Bruk, V.V. Garshenin, and A.I. Kurnosov, *Semiconductor Technology* (Mir Publishers, Moscow, 1971).

Х.А. Елмелігі, З.С. Елманду, Ф. Тагер

ЗМІНА ТИПУ НОСІЇВ У БАГАТОШАРОВИХ
ТОНКИХ ПЛІВКАХ ГРАФЕНУ

Р е з ю м е

Графен має унікальну двовимірну структуру, з великою площею поверхні і значною хімічною стабільністю. Окис графену, отриманий методом Хаммерса, було відновлено до графену із застосуванням імпульсного лазерного напилення. Досліджувалися зразки графену у вигляді порошку і багатошарової структури. Виконано рентгеноструктурний аналіз графену для з'ясування наявності ближнього порядку і визначення числа шарів. Природа ближнього порядку знайдена методами дифракції електронів і просвічуючої електронної мікроскопії. Залежність коефіцієнта Зеєбека від температури свідчить про зміну типу носіїв з *n*-на *p*-тип, починаючи з 60 °С. Вивчено залежність цієї зміни від частоти, напруги і температури. Виявлені осциляції залежності коефіцієнта Зеєбека від товщини відповідають ефекту розмірного квантування в шарах графену. Виміряно і розраховано такі транспортні властивості графену, як швидкість, рухливість і електрична провідність.

Х.А. Элмелиги, З.С. Элманду, Ф. Тагер

СМЕНА ТИПА НОСИТЕЛЕЙ В МНОГОСЛОЙНЫХ
ТОНКИХ ПЛЕНКАХ ГРАФЕНА

Р е з ю м е

Графен обладает уникальной двумерной структурой, большой площадью поверхности и значительной химической стабильностью. Окись графена, полученная методом Хаммерса, была восстановлена до графена с применением импульсного лазерного напыления. Исследовались образцы графена в виде порошка и многослойной структуры. Выполнен рентгеноструктурный анализ графена для выяснения наличия ближнего порядка и определения числа слоев. Природа ближнего порядка найдена методами дифракции электронов и просвечивающей электронной микроскопии. Зависимость коэффициента Зеебека от температуры свидетельствует о смене типа носителей с *n*- на *p*-тип, начиная с 60 °С. Изучена зависимость этой смены от частоты, напряжения и температуры. Обнаруженные осцилляции зависимости коэффициента Зеебека от толщины соответствуют эффекту размерного квантования в слоях графена. Измерены и рассчитаны такие транспортные свойства графена, как скорость, подвижность и электрическая проводимость.